Available online at www.sciencedirect.com
SCIENCE DIRECT®
International Journal of Thermal Sciences 44 (2005) 441–451
International Journal of Thermal Sciences
www.elsevier.com/locate/ijts

Natural convection in tilted square cavities with differentially heated opposite walls

Claudio Cianfrini, Massimo Corcione *, Pier Paolo Dell'Omo

Dipartimento di Fisica Tecnica, Università di Roma "La Sapienza", via Eudossiana, 18, 00184 Rome, Italy

Received 20 January 2004; received in revised form 25 October 2004; accepted 3 November 2004

Abstract

Natural convection in air-filled, tilted square enclosures with two adjacent walls heated and the two opposite walls cooled is numerically studied. A computational model based on the SIMPLE algorithm is used for solving the mass, momentum, and energy transfer governing equations. Simulations are performed for different values of the Rayleigh number in the range $10^4 \leqslant Ra \leqslant 10^6$, and of the tilting angle of the cavity in the range $0° \leqslant \gamma \leqslant 360°$. The influence of Ra and γ on the flow pattern, on the local temperature distribution, and on the heat transfer rates across the enclosure are analysed and discussed. The results obtained for the overall heat transfer in the range of γ between 45° and 225° may be expressed through the semi-empirical dimensionless correlation-equation $Nu = 1.2\,Ra^{0.135}[1 + (\sin\gamma)/2]^{0.405}$. For any tilting angle $\gamma < 45°$, the heat transfer rate is the same as that for angle $(90° - \gamma)$. For any tilting angle $\gamma > 225°$, the heat transfer rate is the same as that for angle $(450° - \gamma)$. In addition, the occurrence of hysteresis phenomena around $\gamma = 45°$ is documented within a range of γ whose extent decreases from nearly 20° to nearly 4° as the Rayleigh number increases from 10^4 to 10^6.

Keywords: Natural convection; Tilted square enclosures; Multidirectional heat flows; Flow transitions

1. Introduction

Most of the studies performed on natural convection heat transfer inside enclosed spaces are related to unidirectional heat flows across rectangular cavities, wherein the buoyancy is induced by imposing a heat flux or a temperature difference either horizontally or vertically from below, in examining conventional convection or thermal instabilities, respectively. Detailed reviews on this topic are easily available in literature, such as those by Ostrach [1] and Bejan [2].

In contrast, while more complex situations are encountered in many practical cases, relatively little work has been carried out for two or three-dimensional heat flows. Among the papers in which the assigned thermal gradient is neither simply horizontal nor vertical, it is worthwhile citing the studies performed by:

(a) Anderson and Lauriat [3], and Ganzarolli and Milanez [4], on enclosures heated from below and cooled along a single side or both sides, respectively;
(b) Aydin et al. [5,6], on cavities heated from one side and cooled from the top;
(c) Shiralkar and Tien [7], who investigated the effects of a simultaneous differential heating of both the horizontal and the vertical walls of a square cavity;
(d) Kirkpatrick and Bohn [8], who carried out heat transfer measurements in a cubical enclosure with different combinations of heated, cooled, and perfectly insulated walls;
(e) Corcione [9], who analysed the effects of the thermal boundary conditions imposed at the sidewalls on natural convection inside square and shallow enclosures heated from below and cooled from above.

However, in the aforementioned works attention has been addressed to the untilted geometry, although the inclination effects may be of interest in many science and engineer-

* Corresponding author. Phone: +39 06 4458 5443, Fax: +39 06 488 0120.
E-mail address: massimo.corcione@uniroma1.it (M. Corcione).

1290-0729/$ – see front matter
doi:10.1016/j.ijthermalsci.2004.11.007

Nomenclature

g	gravity vector	$m\cdot s^{-2}$	
g	gravitational acceleration	$m\cdot s^{-2}$	
k	thermal conductivity of the fluid	$W\cdot m^{-1}\cdot K^{-1}$	
L	width of the cavity	m	
Nu	average Nusselt number		
p	dimensionless pressure		
Pr	Prandtl number, $=\nu/\alpha$		
Q	heat transfer rate	W	
Ra	Rayleigh number, $=g\beta(T_h-T_c)L^3/\alpha\nu$		
t	dimensionless time		
T	temperature	K	
T_0	reference temperature	K	
U	dimensionless velocity component along X-coordinate		
V	dimensionless velocity component along Y-coordinate		
V	dimensionless velocity vector		
x, y	Cartesian coordinates	m	
X, Y	dimensionless coordinates		

Greek symbols

α	thermal diffusivity of the fluid	$m^2\cdot s^{-1}$
β	coefficient of volumetric thermal expansion of the fluid	K^{-1}
γ	tilting angle of the enclosure	deg
ν	kinematic viscosity of the fluid	$m^2\cdot s^{-1}$
θ	dimensionless temperature	
ρ	density of the fluid	$kg\cdot m^{-3}$
Ψ	dimensionless stream function	

Subscripts

c	cold
CX	referred to the cold wall parallel to the x-axis
CY	referred to the cold wall parallel to the y-axis
h	hot
HX	referred to the hot wall parallel to the x-axis
HY	referred to the hot wall parallel to the y-axis
max	maximum value
x	along the x-direction
y	along the y-direction
0	evaluated at the reference temperature

ing applications. In fact, as the buoyancy force components change with orientation, transitions between different flow patterns may occur, and the heat transfer rates may change drastically. In addition, also the effects of the initial conditions on the flow pattern formation should not be neglected, as, e.g., found by Soong et al. [10], who demonstrated the existence of double solutions for differentially heated inclined enclosures.

In this context, the main aim of the present paper is to study the thermal behavior of tilted square enclosures with differentially heated opposite walls, under the assumption that the two temperature differences imposed at the opposite walls are identical.

The study is carried out numerically through a computational code based on the SIMPLE algorithm, which is used for the solution of the mass, momentum and energy transfer governing equations. Simulations are performed for different values of the Rayleigh number Ra in the range between 10^4 and 10^6, and of the tilting angle of the cavity γ in the range between 0° and 360°. The influence of both parameters Ra and γ on the flow pattern, on the local temperature distribution, and on the heat transfer rates across the enclosure are analysed and discussed. The existence of possible multiple solutions is investigated. A dimensionless heat transfer correlation-equation is also given in the paper.

2. Formulation of the problem

An air-filled square enclosure of width L is considered. Two adjacent walls are maintained at temperature T_h, while the two opposite walls are cooled to temperature T_c, as shown in Fig. 1. The coordinate system is defined so that the x-axis is directed along one of the two heated walls, while the y-axis is directed along the other heated wall. The enclosure is tilted at an angle γ with respect to the gravity vector.

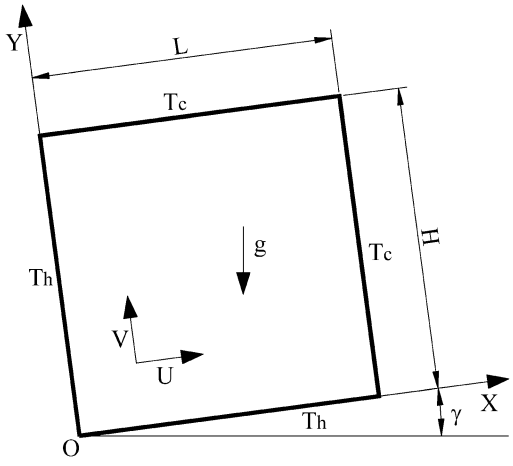

Fig. 1. Sketch of the geometry and coordinate system.

The flow is considered to be two-dimensional and laminar. The fluid is assumed to be incompressible, with constant physical properties and negligible viscous dissipation and pressure work. The buoyancy effects on momentum transfer are taken into account through the Boussinesq approximation.

Once the above assumptions are employed in the conservation equations of mass, momentum, and energy, the

following set of dimensionless governing equations is obtained:

$$\nabla \cdot \mathbf{V} = 0 \tag{1}$$

$$\frac{\partial \mathbf{V}}{\partial t} + (\mathbf{V}\cdot\nabla)\mathbf{V} = -\nabla p + \nabla^2 \mathbf{V} - \frac{Ra}{Pr}\theta\frac{\mathbf{g}}{g} \tag{2}$$

$$\frac{\partial \theta}{\partial t} + (\mathbf{V}\cdot\nabla)\theta = \frac{1}{Pr}\nabla^2\theta \tag{3}$$

where $\mathbf{V}$ is the velocity vector having dimensionless velocity components U and V scaled by ν/L; θ is the dimensionless temperature excess over the mean temperature $T_0 = (T_h + T_c)/2$ scaled by the temperature difference $(T_h - T_c)$; t is the dimensionless time scaled by L^2/ν; p is the dimensionless pressure scaled by $\rho_0\nu^2/L^2$; $\mathbf{g}$ is the gravity vector; Ra is the Rayleigh number; and Pr is the Prandtl number, which is set to 0.71.

The related boundary conditions are $\theta = +0.5$ and $\mathbf{V} = 0$ at the heated walls, and $\theta = -0.5$ and $\mathbf{V} = 0$ at the cooled walls.

Fluid at rest, i.e., $\mathbf{V} = 0$, and uniform temperature $\theta = 0$ across the cavity is assumed as initial condition.

3. Computational procedure

The system of Eqs. (1)–(3) with the boundary and initial conditions stated above is solved through a control-volume formulation of the finite difference method. The pressure–velocity coupling is handled through the SIMPLE algorithm by Patankar and Spalding [11]. The power-law discretization scheme recommended by Patankar [12] is used for the evaluation of the interface convective fluxes. A second-order backward scheme is used for time stepping. Starting from the assigned initial values of the dependent variables, i.e., the assigned initial temperature and velocity fields throughout the enclosure, at each time step the discretized governing equations are solved iteratively through a line-by-line application of the Thomas algorithm. Under-relaxation is used to ensure the convergence of the iterative procedure.

The computational spatial domain is covered with a non-equidistant grid, having a concentration of grid lines near the four walls of the cavity, and a uniform spacing throughout the remaining interior of the cavity. Time discretization is chosen to be uniform. Within each time step, the spatial solution is considered to be fully converged when the maximum absolute values of both the mass source and the percent changes of the dependent variables at any grid-node from iteration to iteration are smaller than prescribed values, i.e., 10^{-3} and 10^{-5}, respectively. Time-integration is stopped when the steady-state solution is reached. This means that the simulation procedure is stopped when the percent difference between the incoming and outgoing heat transfer rates, as well as the percent changes of the primitive variables at any grid-node between two consecutive time-steps, are smaller than prescribed values, i.e., 10^{-4} and 10^{-6}, respectively.

Once the steady-state condition is reached, the average Nusselt numbers of the heated walls Nu_{HX} and Nu_{HY} and those of the cooled walls Nu_{CX} and Nu_{CY}, parallel to the x-axis and to the y-axis, respectively, are calculated using the following expressions:

$$Nu_{HX} = \frac{Q_{HX}}{k(T_h - T_c)} = -\int_0^1 \left.\frac{\partial\theta}{\partial Y}\right|_{Y=0} \mathrm{d}X \tag{4}$$

$$Nu_{HY} = \frac{Q_{HY}}{k(T_h - T_c)} = -\int_0^1 \left.\frac{\partial\theta}{\partial X}\right|_{X=0} \mathrm{d}Y \tag{5}$$

$$Nu_{CX} = \frac{Q_{CX}}{k(T_c - T_h)} = +\int_0^1 \left.\frac{\partial\theta}{\partial Y}\right|_{Y=1} \mathrm{d}X \tag{6}$$

$$Nu_{CY} = \frac{Q_{CY}}{k(T_c - T_h)} = +\int_0^1 \left.\frac{\partial\theta}{\partial X}\right|_{X=1} \mathrm{d}Y \tag{7}$$

where the temperature gradients at the four walls are evaluated by assuming a second-order temperature profile among each wall-node and the next two internal nodes.

It is worth noticing that, for all the geometric-thermal configurations analysed, the following results have been obtained:

$$Nu_{HX} = Nu_{CX} \tag{8}$$

$$Nu_{HY} = Nu_{CY} \tag{9}$$

This means that at the steady-state condition the Nusselt numbers Nu_{HY} and Nu_{CY} may be interpreted as the average Nusselt number Nu_x across the cavity along the x-direction, and that the Nusselt numbers Nu_{HX} and Nu_{CX} may be interpreted as the average Nusselt number Nu_y across the cavity along the y-direction:

$$Nu_x = Nu_{HY} = Nu_{CY} \tag{8a}$$

$$Nu_y = Nu_{HX} = Nu_{CX} \tag{9a}$$

In addition, also the average Nusselt number Nu of the whole enclosure is calculated:

$$Nu = \frac{Q_{HY} + Q_{HX}}{2k(T_h - T_c)} = \frac{1}{2}(Nu_x + Nu_y) \tag{10}$$

Tests on the dependence of the results on both grid-size and time-step have been performed at several Rayleigh numbers for several tilting angles. In particular, the optimal values of mesh spacing and time stepping, i.e., those used for computations, are assumed to be the same as those over which further refinements do not produce any noticeable modification in both the predicted flow field and the heat transfer rates at the steady-state condition. This means when the percent changes of the average Nusselt numbers Nu_x and Nu_y of Eqs. (8a) and (9a), as well as those of the largest values of the velocity components U and V on the two mid-planes of the enclosure, are smaller than prescribed values, i.e., 1 and 2%, respectively.

The number of nodal points and the time-step used for computations lie respectively in the range from 50×50 to 70×70, and in the range from 10^{-5} to 10^{-7}, depending on the Rayleigh number.

Furthermore, in order to validate the numerical code used for the present study, the steady-state solutions obtained as time-asymptotic solutions for an untilted square cavity with differentially heated sidewalls and adiabatic top and bottom walls, have been compared with the benchmark results by de Vahl Davis [13]. In particular, the average Nusselt numbers obtained at Rayleigh numbers in the range between 10^3 and 10^6, and the maximum horizontal and vertical velocity components on the vertical and horizontal midplanes of the enclosure, have been found to be within 1% of the benchmark data. More details on the code validation are available in Cappelli D'Orazio et al. [14].

4. Results and discussion

Numerical simulations are performed for $Pr = 0.71$, which corresponds to air, and for different values of the Rayleigh number in the range $10^4 \leqslant Ra \leqslant 10^6$ and of the tilting angle in the range $0° \leqslant \gamma \leqslant 360°$.

Streamline and isotherm plots are reported in Fig. 2 and in Fig. 3, respectively, for $Ra = 10^6$ and different values of γ in the range from 0° to 360°. The contour lines of the streamline plots correspond to equally-spaced absolute values of the normalized dimensionless stream function $\Psi/|\Psi|_{\max}$ in the range between 0 and 1, where Ψ is defined through $U = \partial\Psi/\partial Y$ and $V = -\partial\Psi/\partial X$. The contour lines of the isotherm plots correspond to equally-spaced values of the dimensionless temperature θ in the range between -0.5 and $+0.5$.

As far as the heat transfer rates are concerned, the distributions of the average Nusselt numbers Nu_x, Nu_y, and Nu versus the tilting angle γ, are reported in Figs. 4–6, for Rayleigh numbers 10^4, 10^5, and 10^6, respectively.

The results obtained may be analysed and discussed as follows.

4.1. Tilting angle in the range between 0° and 90°

At $\gamma = 0°$ the fluid moves clockwise around a relatively stagnant core region at uniform temperature (see Figs. 2(a) and 3(a)).

As the tilting angle increases, the clockwise fluid motion progressively slows down. This is due to the increasing buoyant action driven by the boundary walls HX and CX, which would tend to impose an anticlockwise fluid circulation. In addition, the single-cell flow pattern gets more and more distorted, owing to the progressive enlargement of the quasi-stagnant regions at the bottom and top corners of the enclosure (see Figs. 2(b), (c) and 3(b), (c)).

As γ approaches 45°, the formation of a three-cell flow structure consisting of a clockwise primary cell and two anticlockwise secondary cells, may be observed (see Figs. 2(d) and 3(d)).

For $\gamma > 45°$, the temperature and velocity fields at any tilting angle γ are the same as those corresponding to the tilting angle $(90° - \gamma)$, but specular with respect to the acceleration of gravity, owing to the reversal of the roles played by the boundary walls HX and HY and of the roles played by walls CX and CY (see Figs. 2(e)–(g) and 3(e)–(g)).

It is interesting to note that at $\gamma = 0°$ (and thus at $\gamma = 90°$) the upward-imposed vertical temperature gradient has a destabilizing effect on the temperature and velocity fields which would establish inside the cavity if only the horizontal temperature gradient were provided. This means that the upward-imposed vertical temperature gradient prevents the formation of the vertical thermal stratification typical of cavities with differentially heated sidewalls and perfectly insulated top and bottom walls (see, e.g., Bejan [2]).

As far as the heat transfer rates are concerned, the discussion is here limited to the range of γ between 0° and 45° owing to the aforementioned symmetry of the solutions (see Figs. 4–6).

First, the Nusselt number Nu_y is larger than the corresponding Nusselt number Nu_x. This may be explained by taking into account that for $\gamma < 45°$, owing to the clockwise primary motion, the fluid washing the hot wall HX has been previously cooled by the cold wall CY. This implies that a relatively large amount of heat can be transferred from the wall HX to the fluid, thus leading to relatively high values for Nu_y. In contrast, the fluid washing the hot wall HY has been previously heated by the hot wall HX. This obviously implies that a smaller amount of heat can be transferred from the wall HY to the fluid, with consequent smaller values for Nu_x.

Second, the Nusselt number Nu_y decreases as γ increases. This is a strict consequence of the decrease in strength of the fluid motion discussed above, as well as of the enlargement of the quasi-stagnant regions at both bottom and top corners of the cavity, which imply that the amount of heat exchanged at both walls HX and CX decreases with γ.

Third, the Nusselt number Nu_x remains almost constant as γ increases. In this case it must be noticed that the heat transfer rate at both walls HY and CY is the result of two opposing effects. In fact, as the heat transfer rate at the hot wall HX decreases with γ (see above), also the temperature of the fluid that subsequently washes the hot wall HY decreases with γ, which would imply an increase in the amount of heat exchanged at wall HY. The same kind of consideration applies to the cold wall CY. On the other hand, as the strength of the fluid motion decreases and the extent of the quasi-stagnant regions at the bottom and top corners of the cavity increases with γ, the amount of heat exchanged at both walls HY and CY would tend to decrease as γ increases.

Of course, owing to the cited reversal of the roles played by walls HX and HY and of the roles played by walls CX and CY, abrupt changes in the distributions of both Nusselt numbers Nu_x and Nu_y may be observed as γ exceeds 45°.

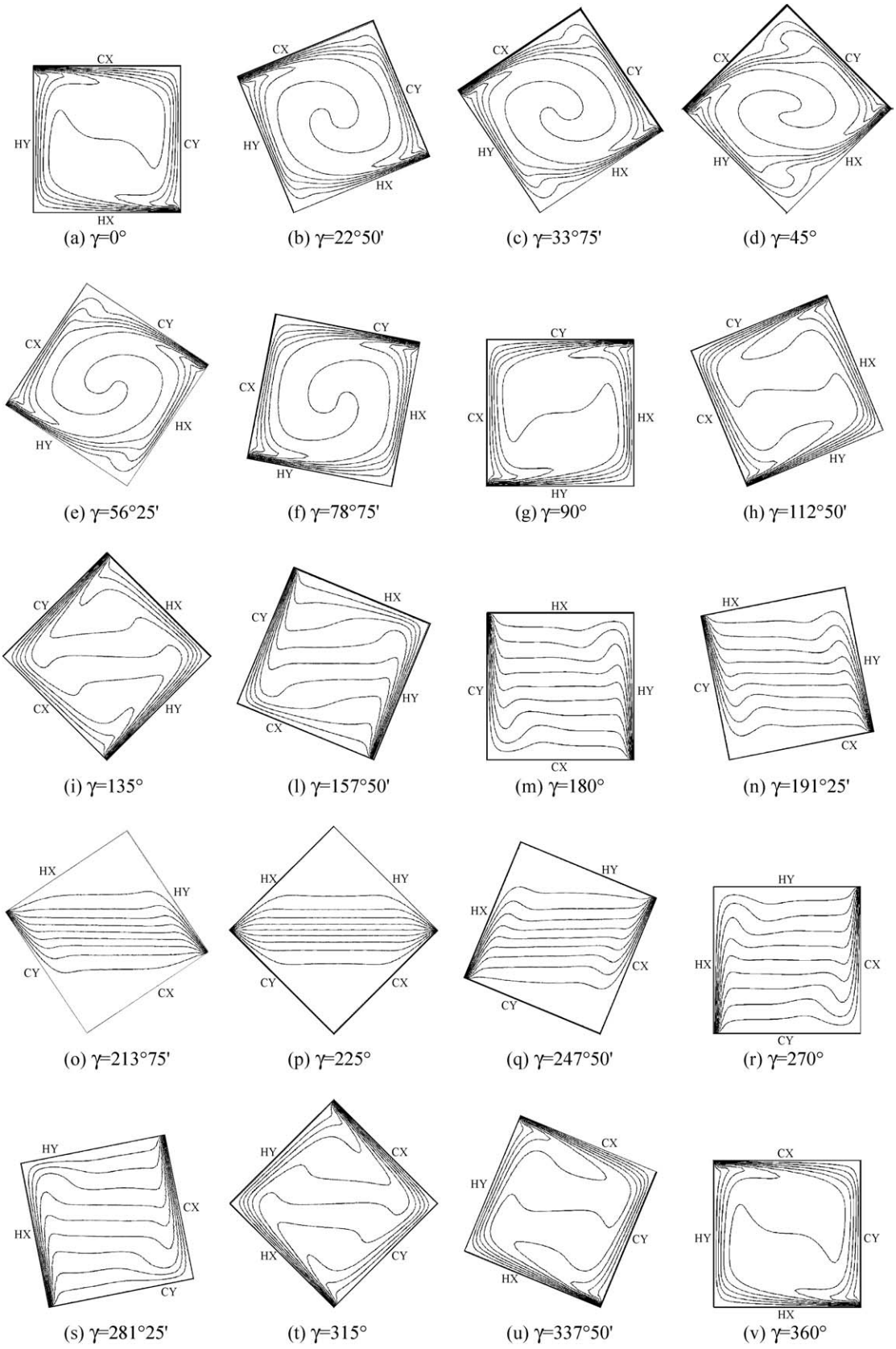

Fig. 2. Steady-state isotherms for $Ra = 10^6$ and different values of γ in the range from 0° to 360°.

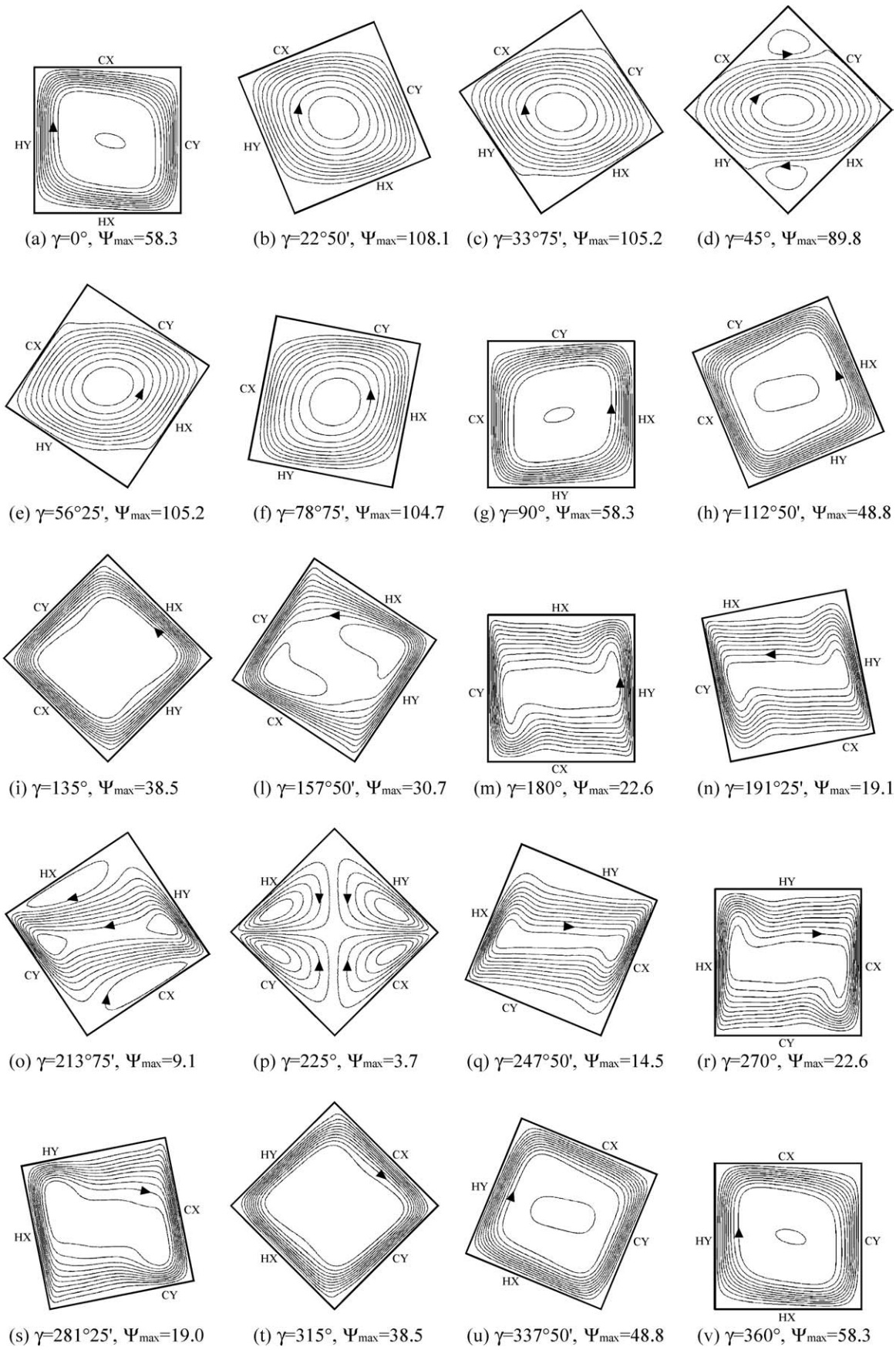

Fig. 3. Steady-state streamlines for $Ra = 10^6$ and different values of γ in the range from 0° to 360°.

4.2. Tilting angle in the range between 90° and 180°

As γ is increased beyond 90° the buoyant action driven by both walls HY and CY adds to that brought about by both walls HX and CX, thus leading to a faster circulation of the fluid (see Figs. 2(h) and 3(h)).

At $\gamma = 135°$ (see Figs. 2(i) and 3(i)) a typical boundary layer motion around a motionless core may be well distinguished. Also the isotherm pattern denotes a core stratification similar to that typical for vertical enclosures with differentially heated sidewalls (see, e.g., Bejan [2]).

In contrast, as γ is further increased above 135°, the strength of the fluid circulation decreases as the thermal driving-force brought about by both walls HX and CX progressively decreases (see Figs. 2(l) and 3(l)).

At $\gamma = 180°$ a pronounced fluid stratification, which derives from the over-stabilizing effect induced by the downward-imposed vertical temperature gradient, may be observed (see Figs. 2(m) and 3(m)).

As far as the heat transfer rates are concerned (see Figs. 4–6), it can be noticed that the Nusselt number Nu_x is larger than the corresponding Nusselt number Nu_y, for exactly the same reason in the range of γ between 0° and 45° the Nusselt number Nu_y is larger than the Nusselt number Nu_x.

In addition, Nu_x undergoes relatively slight changes as γ increases, with a maximum around $\gamma = 135°$, at which the strength of the fluid motion is maximum. In its turn, Nu_y tends to decrease slightly up to $\gamma = 135°$, and then to decrease with a definitely steeper gradient. This may be justified by considering that, for $\gamma < 135°$, the tendency of the heat exchanged at wall HX (or at wall CX) to decrease as the wall faces more and more downwards (or upwards) is partly counterbalanced by the positive effects deriving from the increased fluid motion. In contrast, for $\gamma > 135°$, the negative effects deriving from the fluid motion decrease add to the negative thermal effects deriving from the wall orientation with respect to gravity.

4.3. Tilting angle in the range between 180° and 360°

As γ is increased from 180° to 225° the thermal driving actions delivered by the hot walls HX and HY are in contrast with one another, thus tending to cancel each other out. The same consideration applies to the cold walls. This implies that the fluid circulation progressively slows down with γ (see Figs. 2(n) and 3(n) and Figs. 2(o) and 3(o)).

At $\gamma = 225°$ a practically motionless conductive field is observed (see Figs. 2(p) and 3(p)).

As γ exceeds 225°, the temperature and velocity fields at any tilting angle γ are the same as those corresponding to the tilting angle $(450° - \gamma)$, but specular with respect to the acceleration of gravity, owing to the reversal of the roles played by the boundary walls HX and HY and of the roles played by walls CX and CY (see Figs. 2(q)–(v) and 3(p)–(v)).

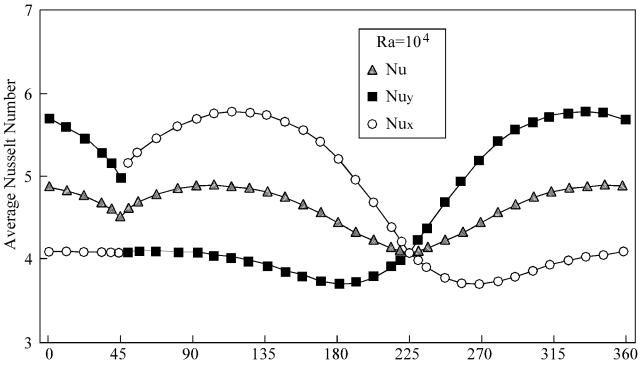

Fig. 4. Steady-state distributions of Nu_x, Nu_y and Nu vs. γ for $Ra = 10^4$.

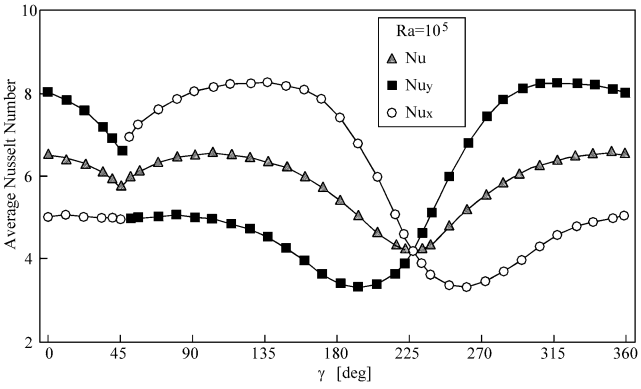

Fig. 5. Steady-state distributions of Nu_x, Nu_y and Nu vs. γ for $Ra = 10^5$.

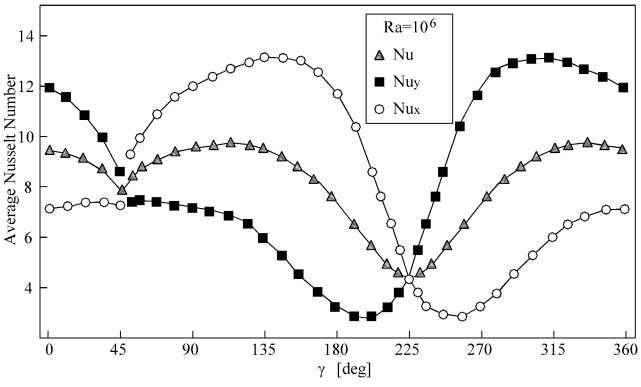

Fig. 6. Steady-state distributions of Nu_x, Nu_y and Nu vs. γ for $Ra = 10^6$.

As far as the overall heat transfer rates are concerned, the discussion is here limited to the range of γ between 180° and 225° owing to the symmetry of the solutions cited above (see Figs. 4–6).

First, it seems interesting to note that at $\gamma = 225°$ both Nu_x and Nu_y reach the same value typical of pure conduction which would derive from the solution of only the equation of energy. Of course, at $\gamma = 225°$ the distribution of the Nusselt number Nu of the whole enclosure has a minimum.

Second, as γ approaches 225°, Nu_x decreases drastically with γ as a strict consequence of the significant decrease in the fluid motion, which is directly responsible for the re-

duced heat transfer rate at the y-oriented walls. In contrast, Nu_y undergoes much smaller changes. In particular, Nu_y increases slightly, thus meaning that in the range $180° \leqslant \gamma < 225°$ the heat transfer at both walls HX and CX is less effective than that for pure conduction.

5. Dimensionless heat transfer correlation-equation

The numerical results obtained for the average Nusselt number of the whole cavity Nu are expressed as a function of a Rayleigh number wherein the characteristic dimension is assumed to be the width L of the enclosure multiplied by a function $f(\gamma)$ of the tilting angle γ. The most suitable empirical expression for $f(\gamma)$ has proved to be $f(\gamma) = 1 + (\sin\gamma)/2$. Thus, the general dimensionless heat transfer correlation-equation is put in the basic form $Nu = A\,Ra^{\alpha}[1 + (\sin\gamma)/2]^{3\alpha}$, where Ra is the Rayleigh number of the enclosure defined in the nomenclature section.

The coefficient A and the exponent α of such correlation have been evaluated through a logarithmic regression of the numerical data in the ranges $10^4 \leqslant Ra \leqslant 10^6$ and $45° \leqslant \gamma < 225°$.

The following semi-empirical dimensionless correlation has been obtained:

$$Nu = 1.2\,Ra^{0.135}\left(1 + \frac{\sin\gamma}{2}\right)^{0.405} \tag{11}$$

with percent standard deviation of error 4.8% and range of percent error from −11 to +12%.

Owing to the symmetry properties of the temperature and velocity fields discussed in the previous section of the paper, for any tilting angle $\gamma < 45°$ the heat transfer rate is the same as that for angle $(90° - \gamma)$, whilst for any tilting angle $\gamma > 225°$ the heat transfer rate is the same as that for angle $(450° - \gamma)$.

6. Occurrence of hysteresis phenomena around $\gamma = 45°$

A search for the occurrence of hysteresis phenomena, i.e., for the existence of possible multiple solutions, each depending on the initial condition assumed, has also been conducted. The search is based on a double computational procedure subdivided into a direct and a reverse course of investigation. In the direct course of investigation the tilting angle γ is progressively increased from 0° to 360° according to a prescribed step-change $\Delta\gamma$, i.e., 1°. In the reverse course of investigation the tilting angle γ is progressively decreased from 360° to 0° with the same $\Delta\gamma$.

In computations where γ is increased, the steady-state temperature and velocity fields for $\gamma = 0°$ are employed as initial condition for the solution of the subsequent inclination angle $\gamma = \Delta\gamma = 1°$, thus beginning a computational sequence in which the steady-state temperature and velocity fields for any given angle γ are the initial condition for the new tilting angle $\gamma + \Delta\gamma$. Once the solution for $\gamma = 360°$ is obtained, the investigation procedure is reversed and the steady-state temperature and velocity fields for any angle γ are the initial condition for the new tilting angle $\gamma - \Delta\gamma$.

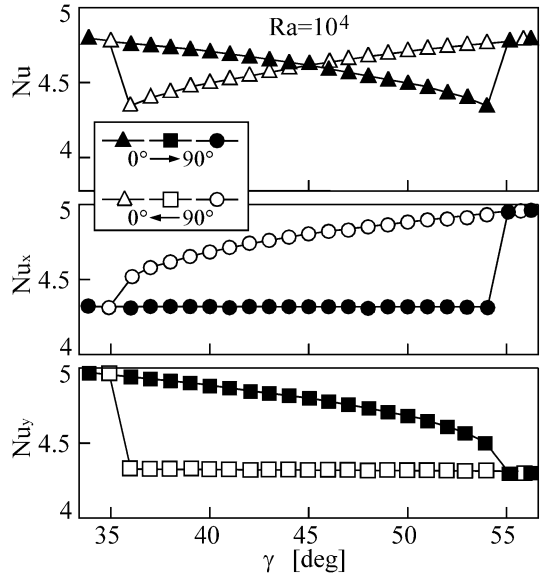

Fig. 7. Hysteresis phenomena around $\gamma = 45°$ denoted by the average Nusselt numbers Nu_x, Nu_y, and Nu for $Ra = 10^4$ (full symbols = γ increasing; empty symbols = γ decreasing).

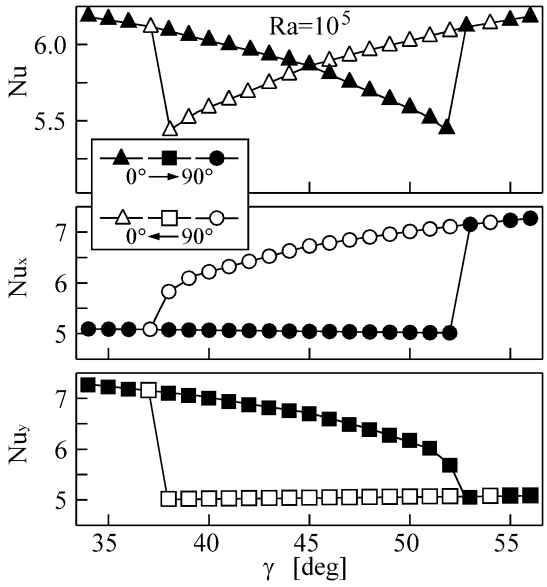

Fig. 8. Hysteresis phenomena around $\gamma = 45°$ denoted by the average Nusselt numbers Nu_x, Nu_y, and Nu for $Ra = 10^5$ (full symbols = γ increasing; empty symbols = γ decreasing).

This type of numerical investigation, based on a two-way sequential procedure as that described above, is very often used whenever the occurrence of hysteresis phenomena, i.e., the existence of multiple solutions, is searched, as, e.g., described in Refs. [10,14].

For the present case, hysteresis phenomena have been found for tilting angles of the cavity around $\gamma = 45°$. The

results obtained are reported in Figs. 7–9, where the distributions of the average Nusselt numbers Nu_x, Nu_y, and Nu are plotted against the tilting angle of the cavity γ, for Rayleigh numbers 10^4, 10^5, and 10^6, respectively. Full symbols correspond to solutions obtained in the direct course of investigation, i.e., when γ is increased. Empty symbols correspond to solutions obtained in the reverse course of investigation, i.e., when γ is decreased.

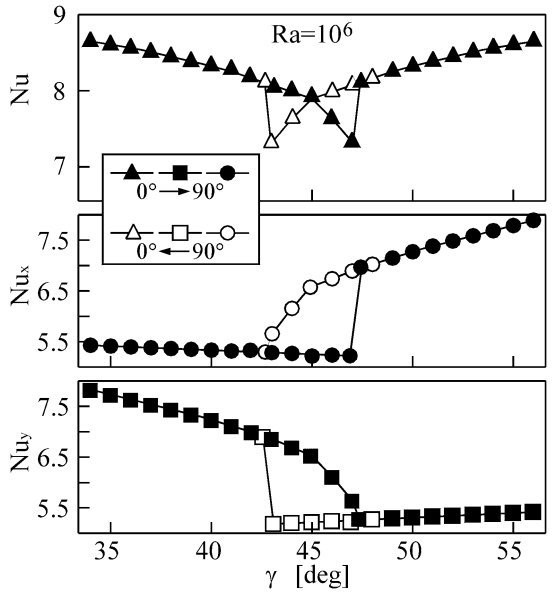

Fig. 9. Hysteresis phenomena around $\gamma = 45°$ denoted by the average Nusselt numbers Nu_x, Nu_y, and Nu for $Ra = 10^6$ (full symbols = γ increasing; empty symbols = γ decreasing).

As far as the direct course of investigation is concerned, it can be observed that for $\gamma = 45° + \Delta\gamma$ the fluid cells move in the same direction of rotation as they do for $\gamma = 45°$, in spite of the reversal of the roles played by the hot walls HX and HY and by the cold walls CX and CY. In fact, as the steady-state temperature and velocity fields for $\gamma = 45°$ (see Figs. 2(d) and 3(d)) are assumed as initial condition for $\gamma = 45° + \Delta\gamma$, the inertia of the clockwise motion of the primary inner cell, and that of the anticlockwise motion of the two secondary cells, prevail over the buoyant action driven by both walls HX and CX (which, in their turn, would tend to impose a reversal in the direction of rotation of the fluid cells). Inertial effects keep on prevailing over the buoyancy effects induced by walls HX and CX even with subsequent tilting angles, up to a critical angle γ_{C1}, at which the flow configuration becomes unstable. For $\gamma = \gamma_{C1}$ (whose value decreases from 55° to 48° as the Rayleigh number increases from 10^4 to 10^6) the thermal effects delivered by both walls HX and CX take over. This implies the transition to a new stable flow configuration, i.e., the reversal in the direction of rotation of the fluid cells.

The transition to the new flow pattern occurs according to the basic time-sequence shown by the eight snapshots of Figs. 10 and 11. Starting from the flow pattern consisting of a clockwise inner cell, and two anticlockwise secondary cells (see Figs. 10(a) and 11(a), corresponding to $\gamma = 47°$), the bottom and top cells get progressively deformed and expand along both walls HX and CX and toward the middle of the enclosure (see Figs. 10(b) and 11(b)). The bottom and top cells keep on expanding, with a consequent progressive compression of the inner cell, which evolves toward a two-

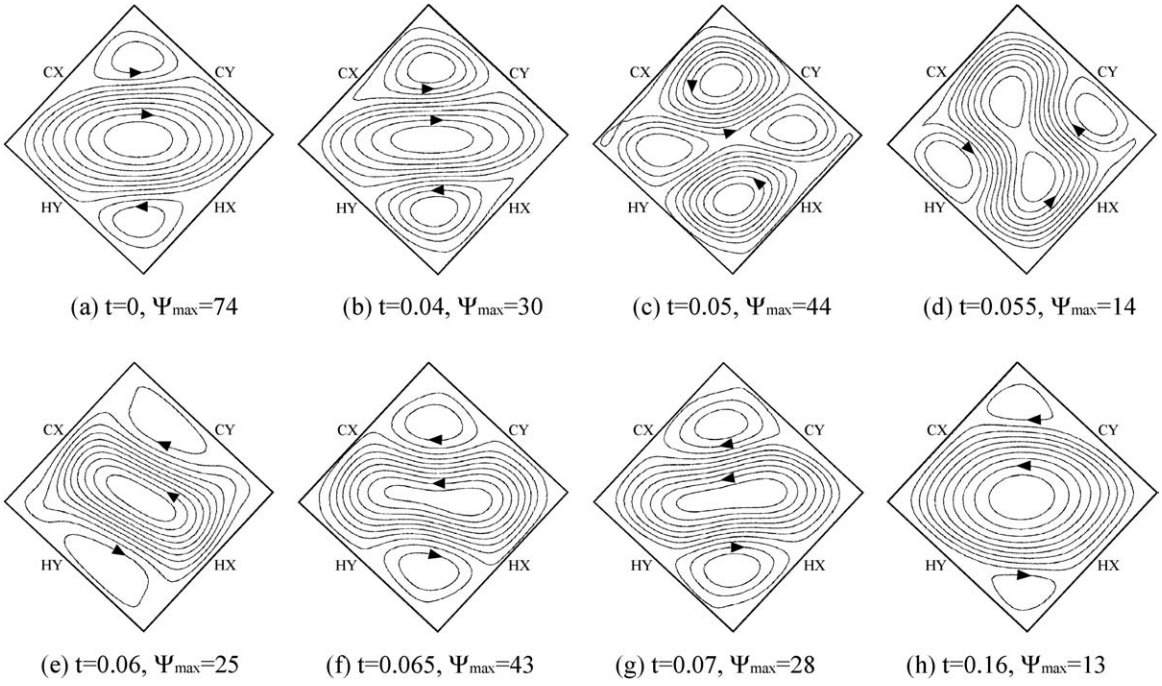

Fig. 10. Time-evolution of the streamlines for $\gamma = \gamma_{C1} = 48°$ and $Ra = 10^6$ from the initial condition (steady-state temperature and velocity fields for $\gamma = 47°$) to the steady-state condition.

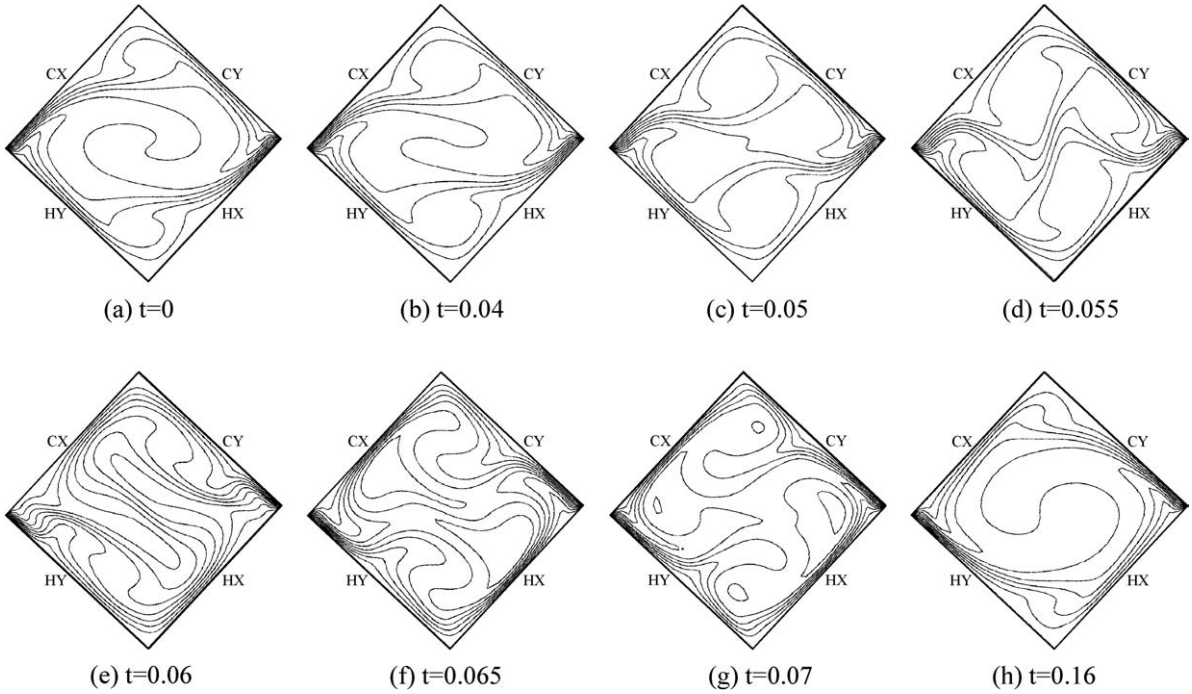

Fig. 11. Time-evolution of the isotherms for $\gamma = \gamma_{C1} = 48°$ and $Ra = 10^6$ from the initial condition (steady-state temperature and velocity fields for $\gamma = 47°$) to the steady-state condition.

in-one flow configuration (see Figs. 10(c) and 11(c)). The bottom and top cells merge, thus implying the formation of a vertical primary cell which rotates anticlockwise and of two counter-rotating secondary side-cells located near the walls HY and CY (see Figs. 10(d) and 11(d)). The whole flow pattern literally rotates around the centre of the cavity (see Figs. 10(e) and 11(e)), up to the achievement of a flow configuration consisting of three cells, stacked on top of each other, whose directions of rotation are exactly the opposite of those of the initial flow pattern (see Figs. 10(f) and 11(f)). The bottom and top cells, and thus the inner cell of the new flow configuration, expand and shrink alternately in time (see Figs. 10(f)–(g) and 11(f)–(g)), up to reaching the new stable flow pattern, which is practically specular to the starting flow pattern with respect to the acceleration of gravity (see Figs. 10(h) and 11(h)).

As expected, the velocity components undergo abrupt modifications as the reversal in the direction of rotation of the fluid cells takes place, as represented in Fig. 12, where the time-distributions of both U and V are reported. In addition, it may be noticed that, as long as the three-cell flow pattern pulsates in time with a decreasing intensity up to the steady-state condition, also the time-distributions of the velocity components oscillate with a decreasing amplitude around the corresponding steady-state value.

As far as the reverse course of investigation is concerned, absolutely similar considerations apply. In particular, the flow transition, i.e., the reversal in the direction of rotation of the fluid cells, occurs at a critical angle γ_{C2} which increases from nearly 35° to nearly 43° as the Rayleigh number increases from 10^4 to 10^6. Thus, around $\gamma = 45°$, in a γ-range

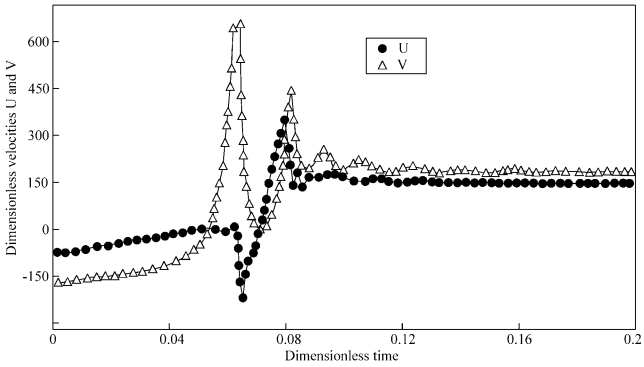

Fig. 12. Time-evolution of the dimensionless velocity components U and V at the internal point $X = 0.7$ and $Y = 0.3$ for $\gamma = \gamma_{C1} = 48°$ and $Ra = 10^6$ from the initial condition (steady-state temperature and velocity fields for $\gamma = 47°$) to the steady-state condition.

whose extent decreases from nearly 20° to nearly 4° as Ra increases from 10^4 to 10^6, the existence of double solutions is documented.

7. Conclusions

Natural convection heat and momentum transfer in air-filled, square enclosures with differentially heated opposite walls, inclined with respect to the gravity vector, has been numerically studied for values of the Rayleigh number Ra in the range between 10^4 and 10^6, and for values of the tilting angle of the cavity γ in the range between 0° and 360°.

The main results of the simulations performed may be summarized as follows:

(a) For a sufficiently wide range of γ around 135° the overall amount of heat transferred along the x-direction across the cavity is larger than that corresponding to the untilted case, i.e., to $\gamma = 0°$; in more details, such enhancement occurs in the range $90° < \gamma < 150°$ for $Ra = 10^4$, in the range $90° < \gamma < 160°$ for $Ra = 10^5$, and in the range $90° < \gamma < 180°$ for $Ra = 10^6$.
(b) For a sufficiently wide range of γ around 315° the overall amount of heat transferred along the y-direction across the cavity is larger than that corresponding to the untilted case, i.e., to $\gamma = 0°$; in more details, such enhancement occurs in the range $300° < \gamma < 360°$ for $Ra = 10^4$, in the range $290° < \gamma < 360°$ for $Ra = 10^5$, and in the range $270° < \gamma < 360°$ for $Ra = 10^6$.
(c) For $\gamma = 225°$, heat transfer across the enclosure occurs for pure conduction.

The results obtained for the overall heat transfer rate in the range of γ between 45° and 225° may be expressed through the semi-empirical dimensionless correlation $Nu = 1.2\,Ra^{0.135}(1 + \sin\gamma/2)^{0.405}$. For any tilting angle $\gamma < 45°$, the heat transfer rate is the same as that for angle $(90° - \gamma)$. For any tilting angle $\gamma > 225°$, the heat transfer rate is the same as that for angle $(450° - \gamma)$.

Moreover, the occurrence of hysteresis phenomena, i.e., the existence of double solutions, around $\gamma = 45°$ is documented within a range of γ whose extent decreases from nearly 20° to nearly 4° as the Rayleigh number increases from 10^4 to 10^6.

References

[1] S. Ostrach, Natural convection in enclosures, J. Heat Transfer 110 (1988) 1175–1190.
[2] A. Bejan, Convection Heat Transfer, second ed., Wiley, New York, 1995.
[3] R. Anderson, G. Lauriat, The horizontal natural convection boundary layer regime in a closed cavity, in: Proceedings of the Eighth International Heat Transfer Conference, San Francisco, CA, vol. 4, 1986, pp. 1453–1458.
[4] M.M. Ganzarolli, L.F. Milanez, Natural convection in rectangular enclosures heated from below and symmetrically cooled from the sides, Internat. J. Heat Mass Transfer 38 (1995) 1063–1073.
[5] O. Aydin, A. Unal, T. Ayhan, Numerical solutions for buoyancy-driven flow in a 2-D square enclosure heated from one side and cooled from above, in: Proceedings of the Advances in Computational Heat Transfer Symposium, Begell House, New York, 1997, pp. 387–394.
[6] O. Aydin, A. Unal, T. Ayhan, Natural convection in rectangular enclosures heated from one side and cooled from the ceiling, Internat. J. Heat Mass Transfer 42 (1999) 2345–2355.
[7] G.S. Shiralkar, L. Tien, A numerical study of the effect of a vertical temperature difference imposed on a horizontal enclosure, Numer. Heat Transfer 5 (1982) 185–197.
[8] A.T. Kirkpatrick, M. Bohn, An experimental investigation of mixed cavity natural convection in the high Rayleigh number regime, Internat. J. Heat Mass Transfer 29 (1986) 69–82.
[9] M. Corcione, Effects of the thermal boundary conditions at the sidewalls upon natural convection in rectangular enclosures heated from below and cooled from above, Internat. J. Thermal Sci. 42 (2003) 199–208.
[10] C.Y. Soong, P.Y. Tzeng, D.C. Chiang, T.S. Sheu, Numerical study on mode-transition of natural convection in differentially heated inclined enclosures, Internat. J. Heat Mass Transfer 39 (1996) 2869–2882.
[11] S.V. Patankar, D.B. Spalding, A calculation procedure for heat, mass and momentum transfer in three-dimensional parabolic flows, Internat. J. Heat Mass Transfer 15 (1972) 1787–1797.
[12] S.V. Patankar, Numerical Heat Transfer and Fluid Flow, Hemisphere, Washington, DC, 1980.
[13] G. de Vahl Davis, Natural convection of air in a square cavity: A bench mark numerical solution, Internat. J. Numer. Methods Fluids 3 (1983) 249–264.
[14] M. Cappelli D'Orazio, C. Cianfrini, M. Corcione, Rayleigh–Bénard convection in tall rectangular enclosures, Internat. J. Thermal Sci. 43 (2004) 135–144.